An inverse boundary element method computational framework for designing optimal TMS coils

Clemente Cobos Sánchez[a], Francisco Javier Garcia-Pacheco[b], Jose Maria Guerrero Rodriguez[a], Justin Robert Hill[c],

[a] *Depto. Ingeniería de Sistemas y Electrónics, Avenida de la Universidad, 10, E-11519, Puerto Real (Cádiz), Spain*
[b] *Depto. de Matemáticas, Avenida de la Universidad, 10, E-11519, Puerto Real (Cádiz), Spain*
[c] *Department of Mathematics, Temple College, Temple, 76504, Texas (USA).*

Abstract

An inverse boundary element method and efficient optimisation techniques were combined to produce a versatile framework to design optimal TMS coils. The presented approach can be seen as an improvement and extension of the work introduced by Cobos Sanchez *et al.* [1] where the optimality of the resulting coil solutions was not guaranteed. This new numerical framework based on a constant boundary element method has been efficiently applied to produce optimal TMS coils with arbitrary geometry, allowing the inclusion of new coil features in the design process, such as optimised maximum current density or reduced temperature. Even the structural properties of the human head were considered using this approach at the design stage to produce more realistic TMS stimulators. Several examples of TMS coils were designed and simulated to demonstrate the validity of the proposed boundary element method approach, and the obtained results show that the described method is an efficient tool for the design of optimal TMS

Email address: clemente.cobos@uca.es (Clemente Cobos Sánchez)

stimulators, which can be applied to a wide range of coil geometries and performance requirements considering the natural variability in the human head properties.

Keywords: Medical device design, Boundary element method, Convex optimisation, TMS, Field synthesis.

---

1. Introduction

Transcranial Magnetic Stimulation (TMS) is a non-invasive technique to stimulate the brain, which is applied to studies of cortical effective connectivity, presurgical mapping, psychiatric and medical conditions, such as major depressive disorder, schizophrenia, bipolar depression, post-traumatic, stress disorder and obsessive-compulsive disorder, amongst others [2].

In TMS, strong current pulses driven through a coil are used to induce an electric field stimulating neurons in the cortex. The efficiency of the stimulation is determined by coil geometry, orientation, stimulus intensity, depth of the targeted tissue and some other factors, such as stimulus waveform and duration.

The TMS stimulator most commonly employed is the so called figure-of-eight or butterfly coil, but since the invention of this technique numerous coil geometries have been proposed to improve the performance and spatial characteristics of the electromagnetic stimulation [3].

The problem in TMS coil design is to find optimal positions for the multiple windings of coils (or equivalently the current density) so as to produce fields with the desired spatial characteristics and properties [4]-[5] (high focality, field penetration depth, low inductance, low heat dissipation, etc.).

In engineering similar problems exist to the one found in TMS coil design, specifically, problems where one needs to determine a quasi-static spatial dis-

tribution of electric currents flowing on a conductive surface subjected to electromagnetic constraints. Some of these problems have been successfully solved by modelling the current under search in terms of the stream function using a boundary element method (BEM). A relevant application can be found in magnetic resonance imaging (MRI), where gradient coils have been efficiently designed following this technique [6, 7].

The first effort to incorporate this numerical strategy to formulate a TMS coil design technique was presented by Cobos Sanchez *et al.* [1], in which a stream-function based current model is incorporated into an inverse boundary element method (IBEM). In that work, the desired current distribution is eventually obtained by solving an optimization problem, one in which a cost function or functional formed with a weighted linear combination of all the objectives, is minimized using classical techniques, such as simple partial derivation.

The computational approach in [1] demonstrated flexibility for the inclusion of new coil features in the design process, such as minimization of the magnetic stored-energy, minimization of power dissipation or minimization of the undesired electric field induced in non target regions of the cortex. Unfortunately, despite the efficiency of the TMS stimulators designed using the stream function IBEM in [1], it was not known how optimal these coil solutions were. Especially since the associated optimisation involved a maximisation problem, which has to be rigorously tackled so as to produce the most effective stimulation of the desired cortex regions.

More recently, Koponen *et al.* [5] have also made use of a stream IBEM to develop another method for designing TMS coils of any desired overall shape and size, where the stored energy and focality can be controlled. Although the stimulators produced in [5] have a remarkable performance, they

exhibit areas of high winding density over the region of stimulation. These dense portions of return windings are associated to high peak temperatures, and may also lead to unpractical designs, specially in TMS coils that are constructed from finite sized wire where there is a minimum wire separation that can be built.
The development of techniques capable of spreading the closest wires would be therefore beneficial to improve the buildability and thermal behaviour of coils designed by using a stream IBEM.

On the other hand, applications of TMS for diagnostic and therapeutic purposes are constantly growing, being often restricted by technical limitations [2]. The ability of the BEM to solve heat [8]-[11] and vibration [12] problems, along with the versatility of stream function based techniques opens up the possibilities of overcoming some of these restrictions with the design of a new generation of TMS stimulators with improved performance and novel properties, such as reduced mechanical stress, minimum coil heating, optimized maximum current density amongst others.
Nonetheless, most of these new performance features increase the mathematical complexity of the TMS coil design, and prompt the need to consider a robust computational framework to rigorously describe the problem and more efficient optimisation techniques, as classical approaches can no longer be straightforwardly applied to handle new non-linear requirements.

In this work, the numerical approach in [1] is improved to produce a computational optimisation framework for designing truly optimal TMS coils of arbitrary shape with novel performance properties such as, for instance, reduced coil heating or optimized current density; the latter is used to illustrate how the buildability of a stimulator designed in [5] can be increased.
Moreover, the suggested method here allows the structural properties of the

human head to be considered in the design process to produce more realistic TMS stimulators.

The presented numerical approach is a combination of general optimisation techniques with a stream function IBEM, which permits the modelling of most of the TMS coil performance features as convex objectives.

The structure of this work is as follows. Firstly an outline of the stream function IBEM is presented in section 2, which leads to the formulation of the TMS coil design problem in section 3. Finally we illustrate the validity of this IBEM approach with the design and performance evaluation of several examples of TMS stimulators of different geometries, which have been chosen to demonstrate the suggested method, to elucidate the behaviour of new TMS coil requirements and how they can be use to improve performance and buildability.

2. Numerical Model

2.1. The current density

A model of the current under search can be achieved by using a constant boundary element method (BEM), that allows the current distribution to be defined in terms of the nodal values of the stream function and elements of the local geometry (see [14]). So let us assume that the surface, $S \subseteq \mathbb{R}^3$, on which we want to find the optimal current, is divided into T triangular flat elements with N nodes, which are lying at each vertex of the element. If we consider the barycenters of the mesh triangles as $\mathbf{R_T} = \{\mathbf{r}_1, \ldots, \mathbf{r}_T\}$, the current density at each element can be written as

$$\begin{array}{rccl} \mathbf{J}: & \mathbf{R_T} \times \mathbb{R}^N & \rightarrow & \mathbb{R}^3 \\ & (\mathbf{r}, \psi) & \mapsto & \mathbf{J}(\mathbf{r}, \psi) \approx \sum_{n=1}^{N} \psi_n \, \boldsymbol{\jmath}^n(\mathbf{r}), \end{array} \tag{2.1}$$

where $\psi = (\psi_1, \psi_2, \ldots, \psi_N)^T$ is the vector containing the nodal values of the stream function and $\boldsymbol{\jmath}^n : \mathbf{R_T} \to \mathbb{R}^3$ are functions related to the curl of the shape functions [14] known as current elements. In the following, $\psi \in \mathbb{R}^N$ is going to be the optimization variable.

If we denote by j_x^n, j_y^n, j_z^n to the Cartesian components of $\boldsymbol{\jmath}^n$, then

$$\mathbf{J}(\mathbf{r}, \psi) \approx \sum_{n=1}^{N} \psi_n \ \boldsymbol{\jmath}^n(\mathbf{r}) = \left(\sum_{n=1}^{N} \psi_n \ j_x^n(\mathbf{r}), \sum_{n=1}^{N} \psi_n \ j_y^n(\mathbf{r}), \sum_{n=1}^{N} \psi_n \ j_z^n(\mathbf{r}) \right)$$

and the absolute current density is $j(\psi) = (j(\mathbf{r}_1, \psi), \ldots, j(\mathbf{r}_T, \psi))^T$ where

$$j(\mathbf{r}, \psi) := \sqrt{\left(\sum_{n=1}^{N} \psi_n \ j_x^n(\mathbf{r}) \right)^2 + \left(\sum_{n=1}^{N} \psi_n \ j_y^n(\mathbf{r}) \right)^2 + \left(\sum_{n=1}^{N} \psi_n \ j_z^n(\mathbf{r}) \right)^2}.$$

The use of this current model allows the discrete formulation of all the magnitudes involved in the problem. An appropriate boundary integral formulation of these magnitudes can be found in Appendix C (5.5), which allows to produce the following matrix equations that transform ψ to the various coil properties and objectives can be then constructed.

2.2. The magnetic field

The magnetic field at a series of H points, $\mathbf{r}_\mathcal{H} = \{\mathbf{r}_1, \mathbf{r}_2, \ldots, \mathbf{r}_H\}$

$$b_{x_i}(\mathbf{r}_\mathcal{H}, \psi) = B_{x_i}(\mathbf{r}_\mathcal{H})\psi, \qquad b_{x_i} \in \mathbb{R}^H, \qquad B_{x_i} \in \mathbb{R}^{H \times N}, \ x_i = x, y, z. \tag{2.2}$$

The coefficient $B_{x_i}(h, n) = b_{x_i}^n(\mathbf{r}_h)$, is the x_i-component of the magnetic induction produced by the current element associated to the n^{th}-node in the prescribed h^{th}-point in $\mathbf{r}_\mathcal{H}$.

2.3. The stored energy in the coil

$$W(\psi) = \psi^T L \psi, \qquad L \in \mathbb{R}^{N\times N}, \tag{2.3}$$

where L is the inductance matrix, which is a full symmetric matrix, and since the amount of stored magnetic energy is always a positive

$$\psi^T L \psi > 0, \qquad \forall \psi \in \mathbb{R}^N, \qquad \psi \neq 0 \tag{2.4}$$

then L is positive definite.

2.4. The resistive power dissipation of the coil

$$P(\psi) = \psi^T R \psi, \qquad R \in \mathbb{R}^{N\times N}. \tag{2.5}$$

where R is the resistance matrix, which is also symmetric and positive-definite. Moreover, the power dissipation can be related to the current at the surface as $R \propto J_x^T J_x + J_y^T J_y + J_z^T J_z$.

2.5. The electric field

The electric field induced in a series of M points inside of the conducting system [7], $\mathbf{r}_{\mathcal{M}} = \{\mathbf{r}_1, \mathbf{r}_2, \ldots, \mathbf{r}_M\}$

$$e_{x_i}(\mathbf{r}_{\mathcal{M}}, \psi) = E_{x_i}(\mathbf{r}_{\mathcal{M}})\psi, \qquad e_{x_i} \in \mathbb{R}^M, \qquad E_{x_i} \in \mathbb{R}^{M\times N},\ x_i = x, y, z. \tag{2.6}$$

where the coefficient $E_{x_i}(h, n)$, is the x_i-component of the electric field induced by the current element associated to the n^{th}-node in the prescribed m^{th}-point in the conducting system $\mathbf{r}_{\mathcal{M}}$. It is worth noting that Eq. (2.6)

can also be used to described the electric field induced in prescribed multi-compartment volume conductor made of different homogeneous sub-domains [15] with different electrical properties, as a representation of a heterogeneous system.

2.6. The temperature

The temperature above ambient of the coil surface [16],

$$t(\mathbf{r}_{\mathbf{R_T}}, \psi) = \Lambda \boldsymbol{\mathcal{C}}(\psi), \qquad t \in \mathbb{R}^T, \qquad \Lambda \in \mathbb{R}^{T \times T}, \qquad \boldsymbol{\mathcal{C}}(\psi) \in \mathbb{R}^T. \tag{2.7}$$

The matrix Λ is defined completely by the geometry of the mesh [16], and $\boldsymbol{\mathcal{C}}$ is a vector containing the constant value of the the Joule heating coefficient at every mesh element

$$\boldsymbol{\mathcal{C}}(l, \psi) = \frac{\rho_r}{k_e w^2} J^2(\mathbf{r}_l, \psi), \qquad \mathbf{r}_l \in \mathbf{R_T}. \tag{2.8}$$

where w is the thickness, k_e the effective thermal conductivity and ρ_r the resistivity of the conducting surface [16].

3. Problem formulation

Cobos Sanchez *et al.* employed the discretized current model presented in section 2 to pose the TMS coil design as an optimization problem, in which a cost function of ψ (that contains terms to control the induced electric and magnetic fields, stored magnetic energy and power dissipation) is minimized by using classical techniques, such as simple partial derivation and subsequent matrix inversion of the consequential system of linear equations. In the following, and for sake of comparison, this type of approach used in [1] will be noted as partial derivation optimisation (PDO). It is also

worth stressing that PDO cannot handle non-linear requirements, such as an optimised maximum current density [6] or optimised maximum temperature, highlighting the need of more adequate optimization techniques.
Moreover, a key issue when designing a TMS coil is to maximise the electric (or magnetic) field induced in the desired cortex target region. In Cobos Sanchez *et al.* work [1], in order to produce maximal stimulation, the stored magnetic energy and/or power dissipation (which can be both seen as smoothing norms of the solution) were minimized for an acceptable level of strength of the electromagnetic fields in the target volume.
Although this scheme has proved to produce TMS coils with efficient performance, it is not clear how optimal these coil solutions were, and especially whether the induced electromagnetic fields were truly maximal in the target region.

Therefore, in order to accurately handle new coil requirements and to guarantee optimality of the resulting solutions, we have to resort to a more mathematically rigorous formulation and approach to the optimisation problem. In this work, it is shown that by using the suggested physical model (Section 2) and after suitable mathematical derivations, the TMS coil design problem can be stated in the form of a convex optimisation. More precisely, all the most relevant design problems can be generally written as

$$\begin{cases} \min f_0(\psi) \\ f_i(\psi) \leq b_i, \quad 1 \leq i \leq m \end{cases} \tag{3.1}$$

where $f_i : \mathbb{R}^n \to \mathbb{R}$ are convex functions for $i = 0, 1, \cdots, m$.

Equation (3.1) represents a quite convenient formulation of the TMS coil design problem, as it can be tackled by using one of the several optimisation packages available for the solution of convex problems. We refer the reader

to Appendix B (5) for a formal and proper mathematical treatment of a multi-objective optimization problem.
In this work, three main optimization schemes have been used to solve problems described by Eq. (3.1)

- Supporting vector analysis [17].
- Particle-swarm optimisation (PSO), an evolutionary technique based on heuristic algorithms [19], where the used characteristics are listed in Appendix A.
- CVX [18], a modelling system for constructing and solving disciplined convex programs.

Moreover, it is also worth stressing that the solution , ψ, of problems described by Eq. (3.1) is the optimal value of the stream function at the conducting surface; the final wire arrangement that approximates the continuous current distribution is produced by contouring ψ [4].

3.1. Forward Problem

Having found the wire pattern, the value of the coil inductance is evaluated by using FastHenry © [20], a multipole impedance extraction tool, and assuming the coil wires have a 1 mm diameter.
Full details of the induced E-field of each TMS coil solution are acquired using an existing direct BEM [7], [15], which allows calculation of the electric field induced by the coil windings in conducting systems.
Moreover, sinusoidal variation of the electric and magnetic fields ($f = 5$kHz) has been adopted, and an arbitrary coil current with peak value of 1 kA has been considered.

Additionally, depth and focality metrics ([1]) were employed to describe the spatial characteristics of the stimulation; where, and unless it is stated, the human head has been modelled by a homogeneous sphere of 8.5 cm radius and isotropic conductivity. The cortical surface was assumed to be at a depth of 1.5 cm from the surface of the head, so the cortex is described by a sphere of 7.0 cm radius.

In the following, we present a set of relevant TMS coil design example cases, which have been chosen to demonstrate the efficiency of the optimisation framework producing truly optimal solutions, and to illustrate its versatility to prototype many different performance requirements and constraints.

For sake of briefness, the coil stimulation is defined by controlling the electric field. Nonetheless, the corresponding formulation in terms of the induced magnetic field can be analogously obtained by interchanging E-field and B-field.

Moreover, due to the similar nature of L and R (both symmetric and positive-definite matrices), results involving the minimum magnetic stored energy TMS coil condition can be straightforwardly exported for the case of designing TMS coils with minimum power dissipation and *vice versa*.

3.2. Minimum stored magnetic energy

In TMS, the brain responds maximally when the induced current is perpendicular to the sulcus [4]. Therefore, it is worth considering the design of TMS stimulator capable of inducing a maximum electric field in a given optimal direction.

So we study the problem of designing a TMS coil with minimum stored energy (inductance) that maximizes one component of the electric field pro-

duced in a target region or region of interest (ROI) formed from a distribution of M points, which can be written

$$\begin{cases} \max \|E\psi\|_2 \\ \min \psi^T L \psi \end{cases} \tag{3.2}$$

where $M, N \in \mathbb{N}$ with $N > M$, $L \in \mathbb{R}^{N\times N}$ and $E \in \mathbb{R}^{M\times N}$, which can be E_x, E_y, E_z or the E-field matrix in any other given direction.

In accordance with Subsection 5.3 of Appendix B (5), Equation (3.2) can be transformed into a more suitable form by taking into account that $L = C^T C$ is the Cholesky decomposition of the inductance matrix L (which is symmetric and positive-definite) and considering a new optimisation variable given by $\tilde{\psi} = C\psi$. We have then the following:

$$\begin{cases} \max \|E\psi\|_2 \\ \min \psi^T L \psi \end{cases} \Leftrightarrow \begin{cases} \max \| \left(EC^{-1}\right) \tilde{\psi}\|_2 \\ \min \|\tilde{\psi}\|_2 \end{cases} \xrightarrow{\text{reform}} \begin{cases} \max \| \left(EC^{-1}\right) \tilde{\psi}\|_2 \\ \|\tilde{\psi}\|_2 = 1 \end{cases}$$

A solution to the last optimization problem is simply a supporting vector of EC^{-1} for the $\|\cdot\|_2$-norm (see Corollary 5.5), which is nothing else but a singular vector associated to the largest singular value of EC^{-1}; that is, any normalized eigenvector associated to the largest eigenvalue of the symmetric matrix $(EC^{-1})^T EC^{-1}$ [17, Theorem 3.3].

3.3. Full field maximization

In this section, we investigate the design of a minimum stored energy TMS coil capable of inducing an electric field with maximum magnitude in a target region formed from a distribution of H points; this particular problem can be formulated as

$$\begin{cases} \max \|E_x\psi\|_2^2 + \|E_y\psi\|_2^2 + \|E_z\psi\|_2^2 \\ \min \psi^T L \psi \end{cases} \tag{3.3}$$

where $M, N \in \mathbb{N}$ with $N > M$, $E_x, E_y, E_z \in \mathbb{R}^{H\times N}$ and $L \in \mathbb{R}^{N\times N}$.

By using again the Cholesky decomposition $L = C^T C$ of the inductance matrix L, and $\tilde{\psi} = C\psi$, problem (3.3) is equivalent to (see Subsection 5.4 of Appendix B (5)):

$$\begin{cases} \max \| \left(E_z C^{-1}\right) \tilde{\psi}\|_2^2 + \| \left(E_y C^{-1}\right) \tilde{\psi}\|_2^2 + \| \left(E_x C^{-1}\right) \tilde{\psi}\|_2^2 \\ \|\tilde{\psi}\|_2 = 1. \end{cases} \tag{3.4}$$

Solving the above problem simply consists of finding the generalized supporting vectors of the matrices $E_z C^{-1}$, $E_y C^{-1}$ and $E_x C^{-1}$. In other words, it suffices to find the normalized eigenvectors associated to the largest eigenvalue of the symmetric matrix $(E_z C^{-1})^T E_z C^{-1} + (E_y C^{-1})^T E_y C^{-1} + (E_x C^{-1})^T E_x C^{-1}$ [17, Theorem 3.3].

It is worth recalling that the magnetic induction (and the electric field for regions with uniform conductivity and no electric charge) is divergence-free field, so the problem of designing a TMS coil that maximises B_x, B_y and B_z fields is not equivalent to one that maximises two components. A full proof of this statement can be found in Subsection 5.5 of Appendix B 5.

3.4. Optimised current

The proposed BEM formulation permits inclusion of the current density in the design process, which can be used to increase the stimulator buildability. For instance, more practical wire patterns can be achieved by controlling the minimum spacing between adjacent wires and by spreading out some of the more closely packed windings. Furthermore, the wire spreading can be used to increase the efficiency of the TMS coil by allowing extra turns to be

added.

To this end, we recall that the minimisation of the l^1-norm of the current density promotes sparsity of the windings, whereas minimising the l^∞-norm causes the wires to become more spread out, and evenly so [6].

The problem of designing a minimum inductance TMS coil with sparse windings or increased minimum wire spacing and capable of stimulating a prescribed region of interest formed with M points can be then written as

$$\begin{cases} \max \|E\psi\|_2 \\ \min \psi^T L \psi + \xi \left\|j(\psi)\right\|_p \end{cases} \tag{3.5}$$

where $p = 1, 2$ or ∞. The weight $\xi \in \mathbb{R}$ is an user-definable regularisation parameter that illustrates the trade-off between coil properties. As it is shown in Subsection 5.2 of Appendix B (5) a solution of Equation (3.5) can be found by solving the following optimisation problem:

$$\min \frac{\psi^T L \psi + \xi \left\|j(\psi)\right\|_p}{\|E\psi\|_2}. \tag{3.6}$$

Additionally, a similar optimisation problem can be set by combining current norms, this can be used to provide coils with favourable characteristics. It has been shown [6] that a mixture of l^1- and l^∞-norm minimisation produces interesting coils whose windings are concentric and compact. This may be of use when constructing coils by hand from fixed cross-section wire because it provides a closer approximation to the real resistance than traditional continuous current density approximations.

3.5. Optimised temperature

Coil temperature is an important issue in the stability of the TMS system and patient comfort. The use of coils with minimised maximum current (Section 3.4) can be a good strategy to tackle this problem, as they

exhibit significantly reduced peak temperatures [6]. Nonetheless, the presented IBEM formalism also allows the coil temperature to be incorporated and controlled in the designed process [16].

The problem of designing a minimum inductance TMS coil with optimised temperature and capable of stimulating a prescribed target ROI formed with M points can be then written as

$$\begin{cases} \max \|E\psi\|_2 \\ \min \psi^T L \psi + \tau \left\|\Lambda \boldsymbol{\mathcal{C}}(\psi)\right\|_p \end{cases} \tag{3.7}$$

where $p = 1, 2$ or ∞. The weight $\tau \in \mathbb{R}$ is an user-definable regularisation parameter that illustrates the trade-off between coil properties. As it is shown in Subsection 5.2 of Appendix B (5) a solution of Equation (3.7) can be found by solving

$$\min \frac{\psi^T L \psi + \tau \|\Lambda \boldsymbol{\mathcal{C}}(\psi)\|_p}{\|E\psi\|_2}. \tag{3.8}$$

Choice of regularization parameter

In the construction of the optimisation problems Eqs. (3.5) and (3.7) we must find the optimal choice of the regularisation parameters ξ and τ. For all the designs tackled here (except Coil 6 and Coil 7), they have been chosen so that the self-inductance, the resistance and temperature above ambient of the TMS coil are less than a prescribed value: $L \leq 10\mu$ H, $R \leq$ 100 mΩ and $T^* \leq 30$ K.

It is worth noting, that this election of maximum values of R, L and T are just illustrative; for each particular problem, the election of the regularisation parameters can be studied so as to yield a solution with a concrete desired coil feature.

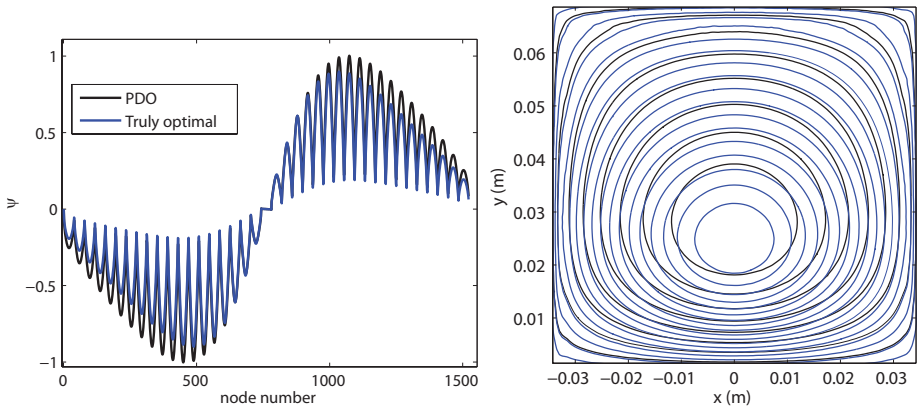

(a) (b)

Figure 1: *a) Optimal stream function values for a rectangular TMS coil described using a mesh of 1681 nodes, designed with singular vector formalism (blue) and PDO (black). b) One quadrant of the wire paths of TMS Coil 1 designed with singular vector formalism (blue) and PDO (black).*

4. Results

4.1. Minimum stored magnetic energy: Coil 1

The first design example considered is referred to as Coil 1, and it is a TMS stimulator of a rectangular flat form of 14 cm $\times$ 7.5 cm located at the xy-plane, and it is designed to maximise B_y in a prescribed region of interest (ROI), which is made up of 400 points inside a spherical region of radius 2 cm that is centred on the z-axis, and 4 cm below the conducting surface. In order to evaluate the optimality of the coil obtained using the suggested approach, we compare it to equivalent one produced using PDO [1].

Figure 1(a) shows the optimal nodal values of the stream function calculated using the supporting vectors formalism (in blue), which are different to those generated with the PDO approach (in black). This discrepancy

can be also found when analysing the wire-paths predicted by both methods Fig. 1(b), and confirmed when evaluating the characteristics of each TMS coil in Table 1, where it can be seen that the TMS stimulator designed with the presented formalism provides a more efficient performance than the counterpart produced with PDO, which has slightly higher values of L.

4.2. Full field maximization: Coil 2

We investigate the design of a minimum inductance spherical TMS coil of radius 9 cm, which is designed to induce an electric field with maximal magnitude in a spherical ROI of 2 cm radius and centred 5 cm above the centre of the conducting sphere. This stimulator is referred to as Coil 2, and the optimal stream function nodal values can be found by using the supporting vectors formalism of the corresponding field matrix; which when contoured produce the wire-paths shown in Fig. 2(a), where red wires indicate reversed current flow with respect to blue ones.

Moreover, for sake of comparison Fig. 2(b) displays one lobe of the wire arrangement of Coil 2 designed with singular vector formalism (blue) and one lobe of the corresponding solution to Coil 2 problem obtained with PDO approach. Although both wire paths are concentrated over the region of stimulation and follow similar pattern, the coil solution produced by PDO is shifted along the azimuthal axis by $\pi/2$ rad with respect to the one predicted by the supporting vectors approach.

The performance parameters of each solution to the spherical TMS Coil 2 problem can be found in Table 1, where it can be seen that although the spatial characteristics of the stimulation are similar there is a significant performance improvement in the inductance of the supporting vectors solution.

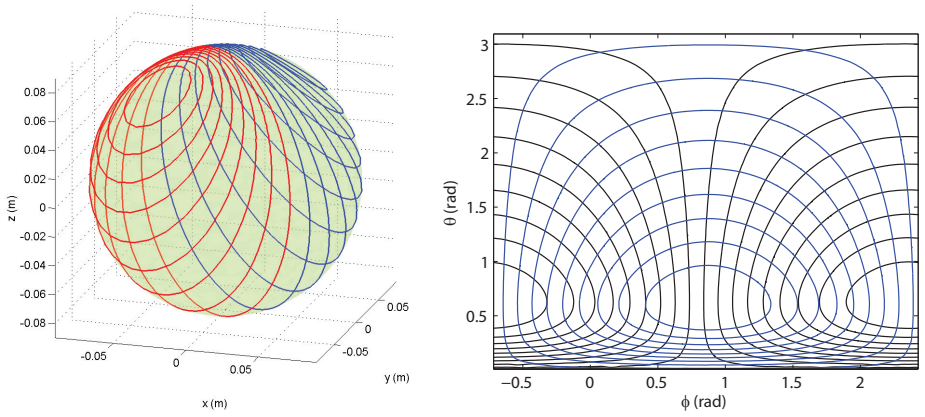

(a) (b)

Figure 2: *a) Optimal stream function values for a spherical TMS coil described using a mesh of nodes, designed with singular vector formalism (blue) and PDO (black). b) One quadrant of the wire paths of TMS coil designed with singular vector formalism (blue) and PDO (black).*

4.3. Realistic target: Coil 3

The proposed framework allows the natural variability in the properties of the human head to be considered in the design process. In order to illustrate this fact, a minimum inductance TMS coil on a hemispherical former of radius 9 cm (Coil 3) has been designed to produce an optimal stimulation in the prefrontal cortex of a human head, which is approximated by a three-compartment scalp-skull-brain model, Fig. 3(a), of conductivities 1, 0.0125 and 1 Sm^{-1}. The scalp, skull and brain are meshed using 7000, 5000 and 3000 elements respectively, as shown in Figs. 3(b)-3(d).

In order to produce the desired stimulation, the TMS coil is designed to maximize the modulus of the electric field, $|\mathbf{E}|$, in a prescribed spherical target region (ROI) of radius 2 cm containing 400 points inside the brain in the frontal lobe, as shown in Fig. 3(a).

Figure 4(a) shows the wire arrangements obtained of Coil 3, which is concentrated over the region of stimulation. It is formed by two lobes of nine turns, which have been produced by contouring the optimal stream function (obtained with the singular vector formalism) with the same number of levels.

In order to evaluate the E-field induced we resort to the direct BEM previously mentioned [7], [15], which allows calculation of the electric field induced by coils in conducting systems. Figures 4(b) and 4(c) show the E-field produced by Coil 3 at the scalp and brain surface respectively; it can be appreciated how the initial requirements of stimulating the frontal cortex are satisfied, as the highest values of the electric field are found in the target ROI.

The relevant parameters for Coil 3 are detailed in Table 1. The depth and focality metrics have not been included, as their values defined in terms spherical homogeneous head model are not appropriated and so they can not be used for comparison to the other TMS stimulators included in this paper.

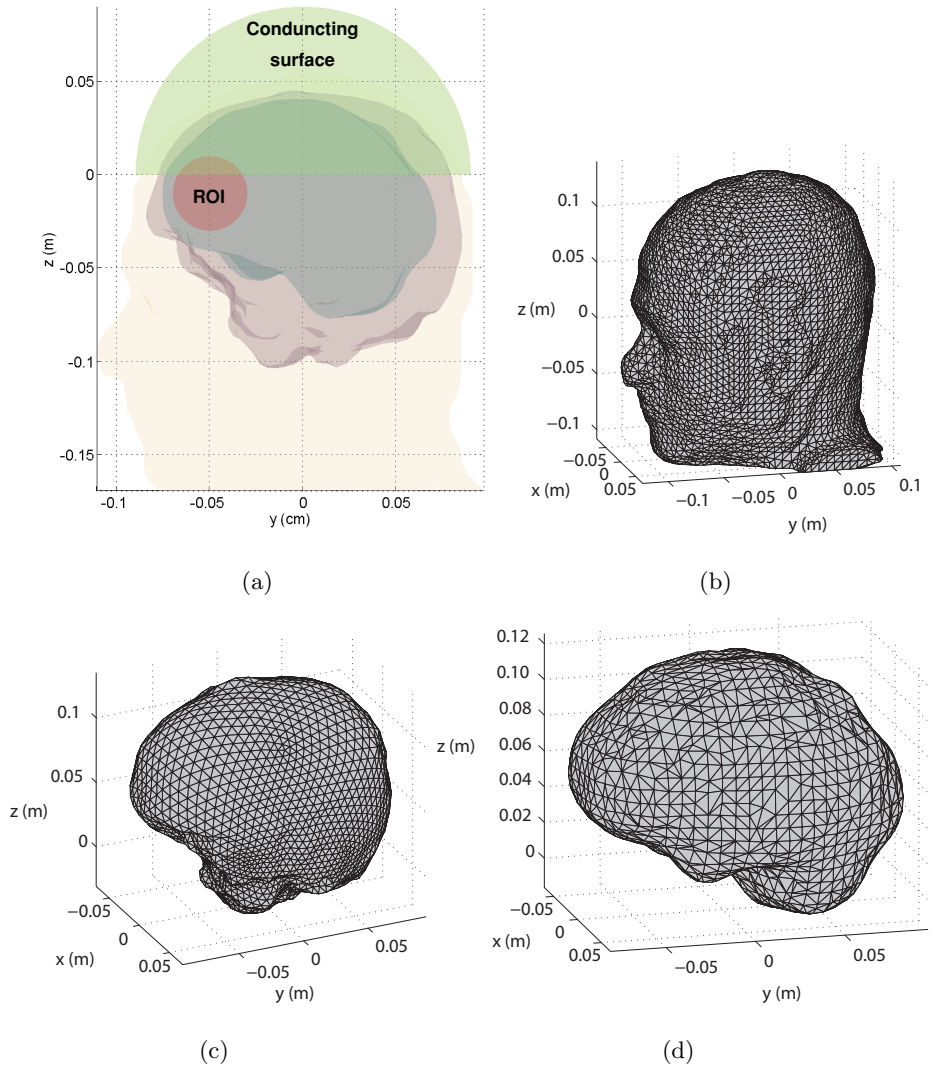

Figure 3: *(a) Description of the three compartment scalp-skull-brain multi-domain along with the spherical region of interest ROI in the prefrontal cortex where the electric field must be maximized, and the hemispherical conducting surface where the Coil 3 is designed; (b) scalp mesh of 9000 elements; (c) skull mesh of 5000 elements; (d) brain mesh of 3000 elements.*

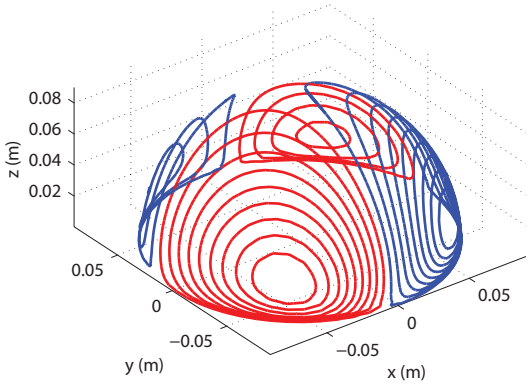

(a)

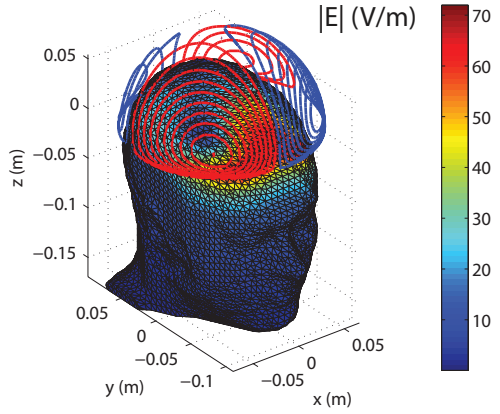

(b)

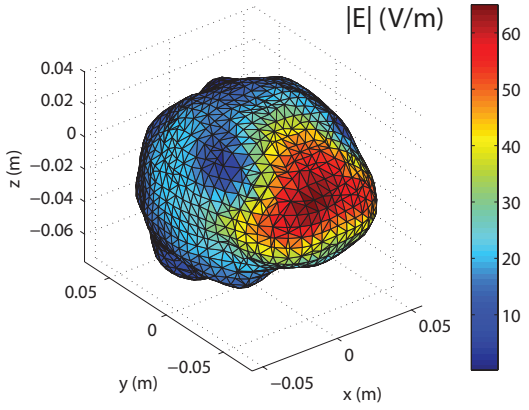

(c)

Figure 4: *(a) Wirepaths with 18 turns of Coil 3 (red wires indicate reversed current flow with respect to blue); (b) E-field modulus induced at the surface of the scalp by Coil 3; (c) E-field modulus induced at the surface of the brain by Coil 3.*

4.4. Optimised current: Coil 4

In this section, the minimisation of the l^∞-norm of the current density is studied for the design of TMS coils with increased minimum wire spacing. So by using the same rectangular flat surface and spherical region of interest (ROI) as in section 4.1, we design a planar stimulator with minimum power dissipation, minimax $|j|$ and capable of inducing maximal electric field in the prescribed target volume of interest (ROI). This stimulator, which is referred to as Coil 4, is shown in Fig. 5(a). It can be appreciated how the minimisation of the l^∞-norm and power dissipation causes the wires to become more spread out and lobes of approximately equally spaced windings. The corresponding performance parameters of Coil 4 can be found in Table 1, where it can be seen an increase in the inductance with respect to Coil 1 due to the augment in the wire spacing.

It is also worth noting that the parameter ξ in Eq. (3.5) has been chosen so that the resistance of the TMS coil is less than 60 mΩ.

4.5. Optimised temperature: Coil 5

Finally, the design of a TMS coil (Coil 5) with reduced hot spot temperatures is studied, where the same rectangular flat surface and spherical target region of interest (ROI) as used in section 4.1 have been employed to produce a stimulator with minimum power dissipation, minimax T and capable of inducing maximal electric field in the ROI.

In order to characterize the temperature at the coil surface, suitable thermal parameters and properties of the conducting former must be considered [16]; in the particular case of the design of Coil 5 the following parameters (section 2.6) have been chosen for the conducting surface : k_e= 0.2 $\mathrm{Wm^{-1}K^{-1}}$, ρ_r= 1.68×10^{-8} Ω m, h_t= 36 W $\mathrm{m^{-2}K^{-1}}$ and w= 35×10^{-6} m.

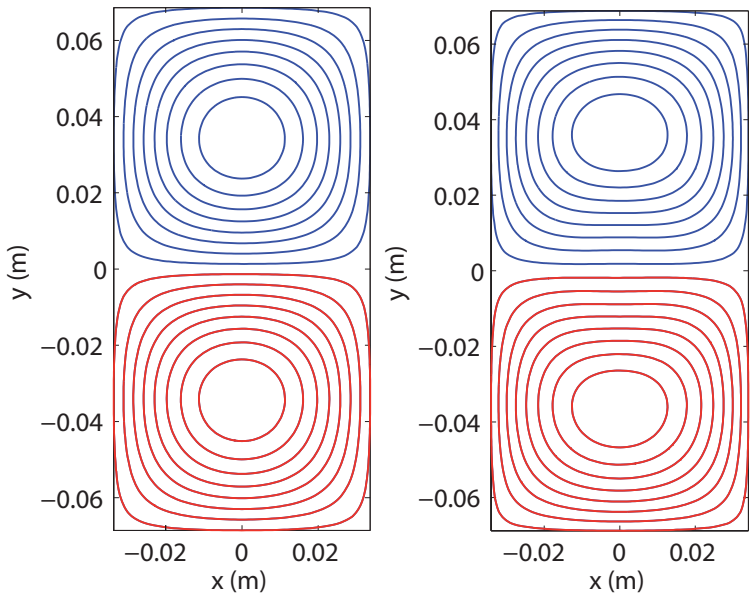

(a) (b)

Figure 5: *(a) Wirepaths with 16 turns of Coil 4; (b) wirepaths with 16 turns of Coil 5. Red wires indicate reversed current flow with respect to blue.*

Figure 5(b) displays the winding pattern of Coil 5 for this particular choice of thermal parameters, where it can be appreciated that the minimization of the l^{∞}-norm of the temperature also causes coil windings to spread out, but not so evenly as in the minimax $|j|$ case (Coil 4, Fig. 5(a)). Again, it can be noted an increase in the inductance with respect Coil 1 due to the increase in the wire spacing.

Additionally, in order to evaluate the reduction of the peak temperature of Coil 5, we can compare its thermal behaviour to the ones exhibited by the other planar TMS coils (Coil 1 and Coil 4). To this end, we resort to the thermal model in [16], which calculates the temperature distribution of coils designed with an inverse IBEM.

Figures 6(a), 6(b) and 6(c) show the colour-coded map of the temperature distribution generated by Coil 1, Coil 4 and Coil 5, respectively.

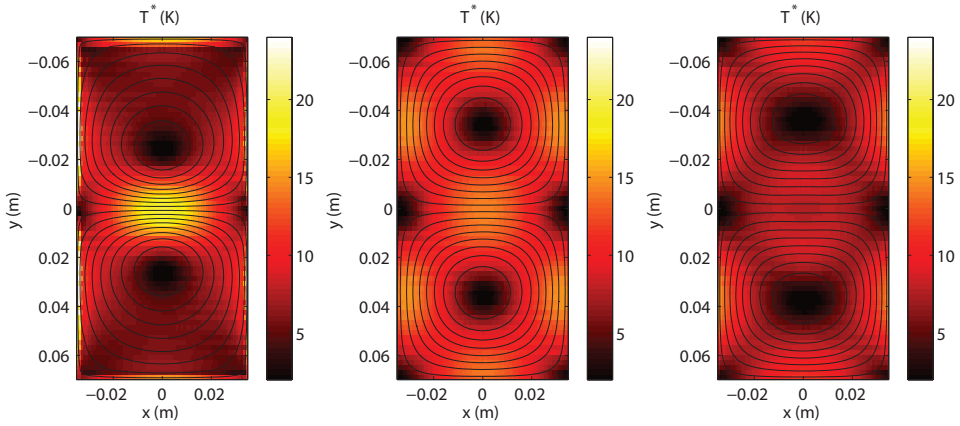

Figure 6: *The temperature above ambient distribution plotted over the surface of the (a) Coil 1, (b) Coil 4 and (c) Coil 5. For all cases the following parameters have been considered: effective thermal conductivity* k_e *=0.2* $Wm^{-1}K^{-1}$*, resistivity of the conducting surface* ρ_r*=1.68*$\times 10^{-8}$ Ω *m, total heat transfer coefficient* h_t*= 36* $W\ m^{-2}K^{-1}$ *and a thickness* w*= 35*$\times 10^{-6}$ *m of the conducting surface.*

The maximum hot spot temperatures occur with a value of 25 K, 21 K and 17 K above ambient temperature, for Coil 1, Coil 4 and Coil 5, respectively. Hence a remarkable 32% drop in the hot spot temperature relative to the environment of Coil 5 with respect to Coil 1. Moreover, in all the three cases the regions with maximum temperature coincide with those where the coil windings are closely spaced, as predicted in [16].

It is also worth noting that the minimax$|j|$ TMS stimulator, Coil 4, also exhibits significantly reduced peak temperatures 6(b), as further spread wires can be expected to help disperse localized regions of joule heating.

Furthermore, the parameter τ in Eq. (3.7) has been chosen so that the

resistance of the TMS coil is less than 60 mΩ.

4.6. Constrained focality: Coil 6

The proposed BEM framework allows the inclusion of optimisation constraints for the spatial characteristics of the stimulation. In order to illustrate this fact and to compare the method with another state of art technique, we tackle the design of the planar (30 cm by 20 cm former) TMS coil in Koponen *et al.* work [5]. This stimulator (Coil 6) must produces a stimulus functionally equivalent to that of the typical figure-of-eight, whilst requiring least stored energy. In our case, each circular lobe of this reference coil has a diameter of 70 mm, containing 10 loops of 1-mm-thick wire. We refer to this stimulator as Coil 0, and its performance parameters are found in Table 1.

The problem of finding Coil can be posed then as

$$\begin{cases} \min \psi^T L \psi \\ \text{subject to } S_{1/2} = S^0_{1/2} \end{cases} \tag{4.1}$$

where $S_{1/2}$ is the focality as defined defined through the effective surface area [3] and $S^0_{1/2}$ is the corresponding focality of the Coil 0.
Here it is also worth mentioning that the constraint in Eq. (4.1) is nonlinear. In [5] it is suitably approximated to a set of linear constraints, but in our case this condition can set straightforwardly in the PSO algorithm.
Figure 7(a) displays the winding pattern of Coil 6, which is equivalent to the optimal planar one designed in [5]. As it can be seen in Table 1, Coil 6 has much lower inductance than the reference figure-of-eight stimulator, Coil 0, while retaining a similar coil-cortex coupling.

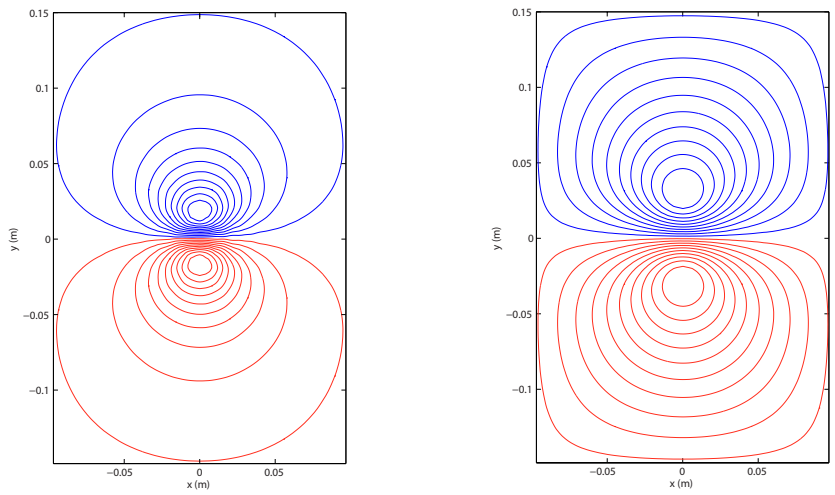

(a) (b)

Figure 7: *(a) Wirepaths with 20 turns of Coil 6; (b) wirepaths with 20 turns of Coil 7. Red wires indicate reversed current flow with respect to blue.*

4.7. Improved buildability: Coil 7

In this section, the benefits and application of the proposed numerical are illustrated by designing a more practical version of Coil 6. In this new stimulator (Coil 7) the minimum spacing between adjacent wires is controlled and some of the more closely packed windings are spread out.

The geometry of Coil 7 is the same as Coil 6, that is, a rectangular flat form of 20 cm $\times$ 10 cm located at the $xy-$plane, and it is designed to produce a stimulus functionally equivalent to Coil 0, with minimum l^1-norm of the current density, and without compromising the magnetic stored energy more

than a 20% of that one corresponding to Coil 6 (W_6). This optimisation problem can be written

$$\begin{cases} \min \|j(\psi)\|_1 \\ \text{subject to } S_{1/2} = S^0_{1/2} \\ \qquad\qquad \psi^T L \psi \leq 1.2 W_6 \end{cases} \tag{4.2}$$

Figure 7(b) shows the wire arrangements obtained of Coil 7, whose windings are more compact, distributed and spread out than those of Coil 6. Additionally, the minimum wire spacing of Coil 7 is higher than that one found in Coil 6. All these facts ease the manufacture of Coil 7, compared to Coil 6.

The price we have to pay for this increment of the minimum wire spacing is the expected increase of the inductance, shown in Table 1, as both Coil 6 and 7 produce stimulations with equivalent spatial characteristics.

Here it is also worth mentioning that by using the same thermal parameters than in Section 4.5, Coil 7 exhibits an improved the temperature above ambient distribution compared to that one produced by Coil 6. More precisely, the hot spot magnitude of Coil 6 is about 34 K, where this peak value decreases up to 28 K for Coil 7.

5. Conclusion

An inverse boundary element method and optimisation techniques were combined to produce an efficient framework to design TMS coils of arbitrary geometry. This approach is an improvement and extension of a previously presented TMS coil design technique [1], in which the optimality of the resulting coil solutions was not guaranteed. The method presented here truly optimises the solution of a given TMS coil design problem, even with the

	L (μH)	R($m\Omega$)	$D_{1/2}$ (cm)	$S_{1/2}$ (cm^2)	N$_{contours}$
Coil 0	16.1	150	1.3	16.0	20
Coil 1 PDO	9.3	70	1.2	13.9	16
Coil 1	7.2	68	1.2	12.7	16
Coil 2 PDO	17.4	174	2.5	48.0	18
Coil 2	14.6	156	2.4	46.9	18
Coil 3	12.3	138	-	-	18
Coil 4	8.6	59	1.3	18.7	16
Coil 5	8.9	58	1.3	18.1	16
Coil 6	9.2	87	1.3	16.0	20
Coil 7	11.0	85	1.3	16.0	20

Table 1: *TMS coil performance parameters:* L *is the inductance,* R *the resistance, $S_{1/2}$ the effective surface area (focality), $D_{1/2}$ the penetration or depth and $N_{contours}$ is the number of levels in which the stream-function is contoured to produce the wire paths. Simulated values of L and R were obtained using FastHenry © [20] using 1 mm diameter circular cross-section wire.*

inclusion of non-linear requirements.

It has been shown that the most relevant TMS coil design problems can be posed as convex optimisations, which here have been efficiently solved employing singular vector analysis and heuristic algorithms.

The suggested method allows the structural properties of the human head to be considered in the design process, which can be used to produce more realistic TMS stimulators. This has been illustrated with the design of a TMS coil that maximizes the electric field induced in the prefrontal cortex

of a human head modelled as a three-compartment scalp-skull-brain heterogeneous conducting system. It is worth noting that the resulting solution strongly depends on the different conductivity values of the multiple domains.

In order to illustrate the versatility of this computational framework, novel requirements and constraints were prototyped, such as minimum coil heating or maximum current density. This new method was used to minimize the l-norms of the current density in a TMS coil to achieve more practical wire patterns. More precisely, it was shown that the minimisation of the l^{∞} and l^{1} norms of the current density and the power dissipation can be used to increase the stimulator buildability by spreading out some of the more closely packed windings.

Although it has been observed that a reduction in TMS coil temperature is possible by minimization of the current density, the presented method can also be used to design stimulators with optimised temperature. This fact was illustrated with the design of a TMS coil for which the temperature in the hottest region of the coil is minimized (minimax T); it displayed up to 32% lower peak temperature when compared to an equivalent minimum inductance TMS coil. The price we have to pay for this temperature reduction is a slight decrease in the spatial characteristics of the electromagnetic stimulation. Nonetheless, this is a considerable improvement which can be especially useful in techniques such as rapid TMS, where coil heating is an important issue.

It is also worth mentioning that it has been found that the winding pattern solution to a given coil design problem involving optimised temperature heavily dependent on the assumed thermal properties of the material.

The numerical procedure that we proposed has been validated by reproduc-

ing results of the state-of-the-art TMS coil design methods such as [5]. It can be also used to extend those existing techniques, as it allows the inclusion of new requirements. Here it has been shown that an increase of the coil inductance can be use to produce more practical coils where the minimum spacing between adjacent wires can be controlled, and some of the more closely packed windings can be spread out.

In this sense, the presented approach can be an useful tool to obtain a comprehensive understanding of the coil design problem, as well as to handle the different coil requirements efficiently and how they should be combined to yield the best solution for a given problem.

[1] Cobos Sanchez, C., Guerrero Rodriguez J. M., Quiros Olozabal A. and Blanco-Navarro D., Novel TMS coils designed using an inverse boundary element method, Physics in Medicine and Biology, Volume 62, Pages 73-90.

[2] Wassermann E. M., Epstein C. M., Ziemann U., Walsh V., Paus T., Lisanby S. H., editors. The Oxford handbook of transcranial magnetic stimulation. New York: Oxford University Press; 2008

[3] Deng Z. D., Lisanby S. H., Peterchev A.V. Electric field depth-focality tradeoff in transcranial magnetic stimulation: simulation comparison of 50 coil designs. Brain Stimul 2013;6:1-13

[4] Koponen L. M., Nieminen J. O., Ilmoniemi R.J. Minimum-energy coils for transcranial magnetic stimulation: application to focal stimulation. Brain Stimul 2014.

[5] Koponen L. M., Nieminen J. O., Mutanen P., Stenroos M., Ilmoniemi

R. Coil optimisation for transcranial magnetic stimulation in realistic head geometry, Brain Stimul., Vol. 10, Issue 4, 2017, Pages 795-805.

[6] Poole M., Jon Shah N. Convex optimisation of gradient and shim coil winding patterns. Journal of Magnetic Resonance, Volume 244, 2014, Pages 36-45.

[7] Cobos Sanchez, C., Gonzalez Garcia S. and Power H. E-coil: an inverse boundary element method for a quasi-static problem, Physics in Medicine and Biology, vol. 55, 3087–3100, 2010.

[8] Kassab AJ, Divo E. A generalized boundary integral equation for isotropic heat conduction with spatially varying thermal conductivity. Eng Anal Bound Elem 1996;18:27386.

[9] Power H. On the existence of Kassab and Divos generalized boundary integral equation formulation for isotropic heterogeneous steady state heat conduction problems. Eng Anal Bound Elem 1997;20:3415.

[10] Bonnet M, Guiggiani M. Comments about the paper entitled "A generalized boundary integral equation for isotropic heat conduction with spatially varying thermal conductivity" by A. J. Kassab and E. Divo. Eng Anal Bound Elem 1998;22:23540

[11] Cvetkovi M, Poljak D, Hirata A, The electromagnetic-thermal dosimetry for the homogeneous human brain model, Engineering Analysis with Boundary Elements, Volume 63, February 2016, Pages 61-73,

[12] Yongtao Yang, Guanhua Sun, Hong Zheng, Application of the 'FE-Meshfree' QUAD4 with continuous nodal stress using radial-polynomial

basis functions for vibration and geometric nonlinear analyses, Engineering Analysis with Boundary Elements, Volume 78, May 2017, Pages 31-48.

[13] Deng Z-D, Lisanby S. H., Peterchev A. V. Electric field depth-focality tradeoff in transcranial magnetic stimulation: simulation comparison of 50 coil designs. Brain Stimul 2013;6:1e13.

[14] Cobos Sanchez, C., S. G. Garcia, L. D. Angulo, C. M. De Jong Van Coevorden, and A. Rubio Bretones. A divergence-free BEM method to model quasi-static currents: Application to MRI coil design. Progress In Electromagnetics Research B, Vol. 20, 187–203, 2010.

[15] Cobos Sanchez C., Power, Garcia S. G., and Rubio Bretones A., Quasi-static multi-domain inverse boundary element method for MRI coil design with minimum induced E-field, Eng.Anal.Bound.Elements, vol. 35, pp. 264–272, 2011.

[16] Cobos Sanchez, C., Guerrero Rodriguez J. M., Quiros Olozabal A. and Poole M., A direct BEM to model the temperature of gradient coils, Engineering Analysis with Boundary Elements, Volume 59, 2015, Pages 159–165.

[17] Cobos Sánchez, C., García-Pacheco F., and Sol Sáez-Martínez, Supporting vectors of continuous linear operators, ANNALS OF FUNCTIONAL ANALYSIS (2017) Accepted. (https://projecteuclid.org/accepted/euclid.afa)

[18] CVX Research, Inc., CVX: Matlab Software for Disciplined Convex Programming, version 2.0, $< http://cvxr.com/cvx >$ (August 2012).

[19] Cobos Sanchez, C., Fernandez Pantoja M. and Gomez Martin R., Design of Gradient Coil for Magnetic Resonance Imaging applying PSO, *IEEE Transaction on Magnetics* , vol. 47, no. 12, pp. 47614768, 2011.

[20] Kamon M Tsuk M J and White J K 1994 FASTHENRY: A Multipole-Accelerated 3-D Inductance Extraction Program *IEEE Transactions on Microwave Theory and Techniques* **42** 1750−1758

[21] Y. Rahmat-Samii and E. Michielssen, *Electromagnetic Optimization by Genetic Algorithms*. New York: Wiley, 1999.

[22] M. Clerc and J. Kennedy, "The particle swarm: Explosion, stability, and convergence in a multidimensional complex space", IEEE Trans Evolutionary Computation 6 (2002), 58-73.

[23] L. Marin, H. Power, R.W. Bowtell, C. Cobos Sanchez, A.A. Becker, P. Glover and I.A. Jones, *Numerical solution for an inverse MRI problem using a regularized boundary element method*, (Special Issue) Engineering Analysis with Boundary Elements 2007.

Appendix A: Particle Swarm Optimization (PSO)

In the present paper, the PSO algorithm uses a swarm population of 20 individuals, a hybrid circle-star neighbourhood, absorbent boundary walls for each dimension, an asynchronous update, and a maximum velocity (at each temporal step) of 20% and 40% of the range of the spatial dimension for longitudinal and transverse designs respectively. The typical parameters in the algorithm [21] are $c1 = c2 = 1.494$ and $\omega = 0.73$, where this particular choice of the algorithm coefficients guarantee system's convergence,

while encouraging exploration [22]. In addition, as a stopping criterion, a maximum number of 2000 generations was used.

Appendix B: Mathematical foundations of the physical models

5.1. Mathematical formulation of a multi-objective optimization problem

The usual notation for the optimization concepts are $\max f$ and $\min f$, which stand for the maximum and the minimum, respectively. A not so usual notation is $\arg\max f$ and $\arg\min f$, which stand for the points at which the maximum value and the minimum value are attained, respectively.

It is well known that an optimization problem is a problem of the form

$$P := \begin{cases} \min f(x) \\ g_i(x) \leq b_i,\ 1 \leq i \leq k \end{cases}$$

where $f, g_1, \ldots, g_k : X \to \mathbb{R}$ are functions defined on a given set X. First off, notice that by switching $-f$ with f we can turn any maximization problem into a minimization one. Two typical sets are associated to P:

- $fea(P) := \{x \in X : g_i(x) \leq b_i\ \forall\ 1 \leq i \leq k\}$, that is, the set of feasible solutions of P.
- $sol(P) := \{x \in fea(P) : f(x) \leq f(y)\ \forall y \in fea(P)\}$, that is, the set of solutions of P.

A multi-objective optimization problem has the form

$$P := \begin{cases} \min f_j(x),\ 1 \leq j \leq l \\ g_i(x) \leq b_i,\ 1 \leq i \leq k \end{cases}$$

where $f_1, \ldots, f_l, g_1, \ldots, g_k : X \to \mathbb{R}$ are functions defined on X. Again, two typical sets are associated to P:

- $fea(P) := \{x \in X : g_i(x) \leq b_i \ \forall \ 1 \leq i \leq k\}$, that is, the set of feasible solutions of P.
- $sol(P) := \{x \in fea(P) : f_j(x) \leq f_j(y) \ \forall y \in fea(P) \ \forall \ 1 \leq j \leq l\}$, that is, the set of solutions of P.

Any multi-objective optimization problem can be re-written as the intersection of optimization problems, that is, if

$$P_j := \begin{cases} \min f_j(x) \\ g_i(x) \leq b_i, \ 1 \leq i \leq k \end{cases}$$

for $1 \leq j \leq l$, then

- $P = P_1 \wedge \cdots \wedge P_l$.
- $fea(P) = fea(P_j)$.
- $sol(P) = sol(P_1) \cap \cdots \cap sol(P_l)$.

In most of the multi-objective optimization problems that we find in this manuscript it occurs that $sol(P) = sol(P_1) \cap \cdots \cap sol(P_l) = \varnothing$. When this happens, the mathematical formulation of the multi-objective optimization problem must be re-defined. A typical reformulation follows:

$$\begin{cases} \min f_j(x), \ 1 \leq j \leq l \\ g_i(x) \leq b_i, \ 1 \leq i \leq k \end{cases} \overset{\text{reform}}{\longrightarrow} \begin{cases} \min f_1(x) \\ f_j(x) \leq c_j, \ 2 \leq j \leq l \\ g_i(x) \leq b_i, \ 1 \leq i \leq k \end{cases}$$

5.2. A particular multi-objective optimization problem

In this subsection we take care of the multi-objective optimization problem

$$M = \begin{cases} \max g(x) \\ \min f(x) \end{cases}$$

where $f, g : X \to (0, \infty)$ are functions and X is a non-empty set. Recall that, in accordance with the previous subsection,

$$sol(M) = \{x \in X : \forall y \in X \ f(x) \leq f(y) \text{ and } g(x) \geq g(y)\} = \arg\max g(x) \cap \arg\min f(x).$$

In case $sol(M) = \varnothing$, an alternative formulation is to look for an optimization problem N whose set of solutions verifies that

$$sol(N) \subseteq \{x \in X : \forall y \in X \text{ either } f(x) \leq f(y) \text{ or } g(x) \geq g(y)\}.$$

The desired problem N is

$$N = \min \frac{f(x)}{g(x)}.$$

Theorem 5.1. *Let X be a non-empty set and consider two functions $f, g : X \to (0, \infty)$. Then*

$$\begin{aligned} \arg\max g(x) \cap \arg\min f(x) &\subseteq \arg\min \frac{f(x)}{g(x)} \\ &\subseteq \{x \in X : \forall y \in X \ \textit{either } f(x) \leq f(y) \ \textit{or } g(x) \geq g(y)\}. \end{aligned}$$

proof

Let $x_0 \in \arg\max f(x) \cap \arg\min g(x)$ and consider any $x \in X$. Notice that $f(x_0) \geq f(x)$ and $g(x_0) \leq g(x)$ by assumption. Therefore

$$\frac{f(x_0)}{g(x_0)} \leq \frac{f(x)}{g(x)}$$

and so

$$x_0 \in \arg\min \frac{f(x)}{g(x)}.$$

On the other hand, assume that

$$x_0 \in \arg\min \frac{f(x)}{g(x)}$$

and fix any arbitrary $x \in X$. If, for instance, $g(x_0) < g(x)$, then

$$f(x_0) = g(x_0)\frac{f(x_0)}{g(x_0)} < g(x)\frac{f(x_0)}{g(x_0)} \leq g(x)\frac{f(x)}{g(x)} = f(x).$$

In virtue of the previous theorem, we have that

$$\begin{cases} \max g(x) \\ \min f(x) \end{cases} \xrightarrow{\text{reform}} \quad \min \frac{f(x)}{g(x)}$$

5.3. The previous multi-objective optimization problem in the scope of matrices

A particular case of the previous multi-objective optimization problem is the one described in Equation (3.2), which has the form

$$\begin{cases} \max \|A\varphi\| \\ \min \|\varphi\| \end{cases}$$

where A is an $H \times N$ matrix, $\varphi \in \mathbb{R}^N$ and $\|\cdot\|$ is a norm in $\mathbb{R}^N$. The following lemma shows that the previous multi-objective optimization problem does not have a solution and thus it must be reformulated according to Theorem 5.1.

Lemma 5.2. *Let A be an $H \times N$ matrix and consider a norm $\|\cdot\|$ in $\mathbb{R}^N$. There does not exist $\varphi \in \mathbb{R}^N$ such that, for all $\psi \in \mathbb{R}^N$, $\|A\varphi\| \geq \|A\psi\|$ and $\|\varphi\| \leq \|\psi\|$.*

Proof

Suppose to the contrary that there is $\varphi \in \mathbb{R}^N$ such that $\|A\varphi\| \geq \|A\psi\|$ and $\|\varphi\| \leq \|\psi\|$ for all $\psi \in \mathbb{R}^N$. Since $\|\varphi\| \leq \|\psi\|$ for all $\psi \in \mathbb{R}^N$ we must have that $\varphi = 0$ which then contradicts that $\|A\varphi\| \geq \|A\psi\|$ for all $\psi \in \mathbb{R}^N$ since $A\varphi = 0$.

In accordance with the previous subsection, it is precise to apply the following reformulation:

$$\begin{cases} \max \|A\varphi\| \\ \min \|\varphi\| \end{cases} \xrightarrow{\text{reform}} \quad \min \frac{\|\varphi\|}{\|A\varphi\|}.$$

In order to solve $\min \frac{\|\varphi\|}{\|A\varphi\|}$, we must rely on the supporting vectors of A.

Definition 5.3 (Supporting vector). *Let X and Y be Banach spaces and consider a continuous linear operator $T : X \to Y$.*

- *The norm of T is defined as $\|T\| := \sup\{\|T(x)\| : \|x\| = 1\}$.*
- *The set of supporting vectors of T is $\operatorname{suppv}(T) := \{x \in X : \|x\| = 1$ and $\|T(x)\| = \|T\|\}$.*

We refer the reader to [17] for a wide perspective on the topological and geometrical structure of the set $\operatorname{suppv}(T)$.

Theorem 5.4. *Let X and Y be Banach spaces and consider a non-zero continuous linear operator $T : X \to Y$. Then*

1. $\operatorname{suppv}(T) = \arg\min\{\|x\| : \|T(x)\| = \|T\|\}$ *and* $\min\{\|x\| : \|T(x)\| = \|T\|\} = 1$.
2. $\arg\min \frac{\|x\|}{\|T(x)\|} = \bigcup_{t>0} t\operatorname{suppv}(T)$.

Proof

1. Let $x_0 \in \operatorname{suppv}(T)$ and consider any $y \in X$ with $\|T(y)\| = \|T\|$. Notice that
$$\frac{\|T\|}{\|y\|} = \left\| T\left(\frac{y}{\|y\|}\right) \right\| \leq \|T\|$$

therefore $\|x_0\| = 1 \leq \|y\|$. Conversely, let $x_0 \in \arg\min\{\|x\| : \|T(x)\| = \|T\|\}$. All we need to show is that $\|x_0\| = 1$. Notice that $\|T\| = \|T(x_0)\| \leq \|T\|\|x_0\|$, therefore $\|x_0\| \geq 1$. Assume that $\|x_0\| > 1$. Let $y \in X$ with $\|y\| = 1$ such that $\|T(y)\|$ is sufficiently close to $\|T\|$ to obtain that $\frac{\|T\|}{\|T(y)\|} < \|x_0\|$. In this situation, note that $\left\|T\left(\frac{\|T\|y}{\|T(y)\|}\right)\right\| = \|T\|$ thus

$$\|x_0\| \leq \left\|\frac{\|T\|y}{\|T(y)\|}\right\| = \frac{\|T\|}{\|T(y)\|} < \|x_0\|,$$

which is a contradiction. As a consequence, $\|x_0\| = 1$ and by definition $x_0 \in \text{suppv}(T)$.

2. Let $x_0 \in \bigcup_{t>0} t\text{suppv}_{\|\cdot\|}(T)$ and write $x_0 = t_0 z_0$ for some $t_0 > 0$ and $z_0 \in \text{suppv}(T)$. We will show that $x_0 \in \arg\min \frac{\|x\|}{\|T\varphi\|}$. Indeed, let $y \in X \setminus \ker(T)$. Then

$$\frac{\|x_0\|}{\|T(x_0)\|} = \frac{\|t_0 z_0\|}{\|T(t_0 z_0)\|} = \frac{\|z_0\|}{\|T(z_0)\|} = \frac{1}{\|T\|} \leq \frac{1}{\left\|T\left(\frac{y}{\|y\|}\right)\right\|} = \frac{\|y\|}{\|T(y)\|}.$$

Conversely, let $x_0 \in \arg\min \frac{\|x\|}{\|T(x)\|}$. We will show that $\frac{x_0}{\|x_0\|} \in \text{suppv}(T)$, and so $x_0 = \|x_0\|\frac{x_0}{\|x_0\|} \in \|x_0\|\text{suppv}(T) \subseteq \bigcup_{t>0} t\text{suppv}_{\|\cdot\|}(T)$. Indeed, let $y \in X$ with $\|y\| = 1$. Note that

$$\frac{1}{\left\|T\left(\frac{x_0}{\|x_0\|}\right)\right\|} = \frac{\|x_0\|}{\|T(x_0)\|} \leq \frac{\|y\|}{\|T(y)\|} = \frac{1}{\left\|T\left(\frac{y}{\|y\|}\right)\right\|},$$

therefore $\left\|T\left(\frac{x_0}{\|x_0\|}\right)\right\| \geq \|T(y)\|$ and thus $\left\|T\left(\frac{x_0}{\|x_0\|}\right)\right\| = \|T\|$.

Note that the above concepts make sense in the scope of matrices since they can be seen as continuous linear operators between finite dimensional real vector spaces. Therefore we have the following immediate corollary.

Corollary 5.5. *Let A be an $H \times N$ matrix and consider a norm $\|\cdot\|$ in $\mathbb{R}^N$. Then*

1. $\operatorname{suppv}(A) = \arg\min\{\|\varphi\| : \|A\varphi\| = \|A\|\}$ *and* $\min\{\|\varphi\| : \|A\varphi\| = \|A\|\} = 1$.
2. $\arg\min \frac{\|\varphi\|}{\|A\varphi\|} = \bigcup_{t>0} t\operatorname{suppv}(A)$.

The previous corollary gives us the hint to refine a bit more the reformulation provided in the previous subsection:

$$\left\{\begin{array}{l}\max\|A\varphi\| \\ \min\|\varphi\|\end{array}\right. \overset{\text{reform}}{\longrightarrow} \left\{\begin{array}{l}\min\frac{\|\varphi\|}{\|A(\varphi)\|} \\ \|\varphi\| = 1\end{array}\right. \Leftrightarrow \left\{\begin{array}{l}\max\|A\varphi\| \\ \|\varphi\| = 1\end{array}\right. \Leftrightarrow \left\{\begin{array}{l}\min\|\varphi\| \\ \|A\varphi\| = \|A\|\end{array}\right.$$

5.4. A change of variable in the previous multi-objective optimization problem

It is a trivial fact that $fea(P) = \phi(fea(Q))$ and $sol(P) = \phi(sol(Q))$ where

$$P := \left\{\begin{array}{l}\min f_j(x),\ 1 \le j \le l \\ g_i(x) \le b_i,\ 1 \le i \le k\end{array}\right. , \quad Q := \left\{\begin{array}{l}\min(f_j \circ \phi)(y),\ 1 \le j \le l \\ (g_i \circ \phi)(y) \le b_i,\ 1 \le i \le k\end{array}\right.$$

and $\phi : Y \to X$ is a bijection. In this setting, ϕ is called a change of variables in the multi-objective optimization problem. In the scope of matrices, a suitable change of variables is very helpful and will be mostly used.

Another trivial fact is that $fea(P) = fea(Q)$ and $sol(P) = sol(Q)$ where

$$P := \left\{\begin{array}{l}\min f_j(x),\ 1 \le j \le l \\ g_i(x) \le b_i,\ 1 \le i \le k\end{array}\right. , \quad Q := \left\{\begin{array}{l}\min(\phi_j \circ f_j)(x),\ 1 \le j \le l \\ (\chi_i \circ g_i)(x) \le \chi_i(b_i),\ 1 \le i \le k\end{array}\right.$$

and $\phi_j, \chi_i : \mathbb{R} \to \mathbb{R}$ are strictly increasing for $1 \le j \le l$ and $1 \le i \le k$.

Lemma 5.6. *If L is a $N \times N$ symmetric and positive-definite matrix, then there exists an invertible $N \times N$ matrix C such that $\psi^T L\psi = \|C\psi\|_2^2$ for all $\psi \in \mathbb{R}^N$.*

Proof

We will provide two different proofs:

1. Since L is symmetric and positive-definite, we can appeal to the Cholesky decomposition of L, that is, $L = C^T C$. Indeed, notice that

$$\psi^T L \psi = \psi^T (C^T C) \psi = (C\psi)^T (C\psi) = \|C\psi\|_2^2 .$$

2. Consider the bilinear map $(\varphi, \psi)_L := \varphi^T L \psi$. Since L is symmetric and positive-definite, this bilinear map defines a scalar product which makes $\mathbb{R}^N$ become a Hilbert space whose norm is $\|\varphi\|_L := (\varphi, \varphi)_L^{\frac{1}{2}} = \sqrt{\varphi^T L \varphi}$. Since all the Hilbert spaces of the same dimension are linearly isometric, there exists a surjective linear isometry $T : \left(\mathbb{R}^N, \|\cdot\|_L\right) \to \left(\mathbb{R}^N, \|\cdot\|_2\right)$. If denote by C to the matrix associated to the isometry T, then

$$\|C\psi\|_2^2 = \|T(\psi)\|_2^2 = \|\psi\|_L^2 = \psi^T L \psi$$

for all $\psi \in \mathbb{R}^N$.

Observe that the condition $\psi^T L \psi = \|C\psi\|_2^2$ for all $\psi \in \mathbb{R}^N$ automatically implies that C is invertible. Indeed, since C is a square matrix it suffices to show that is kernel is null. So let $\psi \in \ker(C)$. Then $\psi^T L \psi = \|C\psi\|_2^2 = 0$, which implies that $\psi = 0$ since L is positive-definite.

By relying on the previous lemma and by taking into account the previous two facts, we can state the following chain of implications:

$$\left\{ \begin{array}{l} \max \|A\psi\|_2 \\ \min \psi^T L \psi \end{array} \right. \Leftrightarrow \left\{ \begin{array}{l} \max \|A\psi\|_2 \\ \min \sqrt{\psi^T L \psi} \end{array} \right. \Leftrightarrow \left\{ \begin{array}{l} \max \|A\psi\|_2 \\ \min \|C\psi\|_2 \end{array} \right. \Leftrightarrow \left\{ \begin{array}{l} \max \|(AC^{-1})\varphi\|_2 \\ \min \|\varphi\|_2 \end{array} \right.$$

Observe that the last multi-objective optimization problem has the form treated in Subsection 5.3 and thus it can reformulated as explained in Corollary 5.5.

5.5. Operators with null divergence

Contrary to what many physicists think, there can be found magnetic fields with null divergence with the property that optimizing jointly all components is not equivalent to optimizing jointly some components.

Fix $N \in \mathbb{N}$ and let $b^n : \mathbb{R}^3 \to \mathbb{R}^3$ be vector fields for every $1 \leq n \leq N$. If $\psi = (\psi_1, \ldots, \psi_N)^T \in \mathbb{R}^N$, then the vector field

$$B := \sum_{n=1}^{N} \psi_n b^n$$

verifies that

$$\mathrm{div}(B) = \sum_{n=1}^{N} \psi_n \mathrm{div}(b^n).$$

Now fix $H \in \mathbb{N}$ with $H < N$ and $r_1, \ldots, r_H \in \mathbb{R}^3$. We can define now the following linear operators $B_x, B_y, B_z : \mathbb{R}^N \to \mathbb{R}^H$ by

$$B_x(\psi) := \left(\sum_{n=1}^{N} \psi_n b_x^n(r_1), \ldots, \sum_{n=1}^{N} \psi_n b_x^n(r_H) \right)$$

$$B_y(\psi) := \left(\sum_{n=1}^{N} \psi_n b_y^n(r_1), \ldots, \sum_{n=1}^{N} \psi_n b_y^n(r_H) \right)$$

$$B_z(\psi) := \left(\sum_{n=1}^{N} \psi_n b_z^n(r_1), \ldots, \sum_{n=1}^{N} \psi_n b_z^n(r_H) \right)$$

where b_x^n, b_y^n, b_z^n are the components of the vector field b^n for $1 \leq n \leq N$. Notice that the three linear operators above can be seen as $H \times N$ matrices.

We will disprove the equivalence of the following optimization problems when $\mathrm{div}(B) = 0$:

$$\left\{\begin{array}{l}\max \|B_x\psi\|_2^2+\|B_y\psi\|_2^2+\|B_z\psi\|_2^2\\ \|\psi\|_2=1,\ \psi\in\mathbb{R}^N\end{array}\right. \Leftrightarrow \left\{\begin{array}{l}\max \|B_x\psi\|_2^2+\|B_y\psi\|_2^2\\ \|\psi\|_2=1,\ \psi\in\mathbb{R}^N\end{array}\right.$$

Example 5.7. *Indeed, it suffices to consider constant vector fields* $b^n(r) := (b_1^n, b_2^n, b_3^n)$ *for all* $r \in \mathbb{R}^3$ *and* $1 \leq n \leq N$. *It is clear that* $\operatorname{div}(b^n) = 0$ *for* $1 \leq n \leq N$ *and thus* $\operatorname{div}(B) = 0$. *Observe that*

$$B_x = \begin{pmatrix} b_1^1 & b_1^2 & \cdots & b_1^N \\ b_1^1 & b_1^2 & \cdots & b_1^N \\ \vdots & \vdots & \ddots & \vdots \\ b_1^1 & b_1^2 & \cdots & b_1^N \end{pmatrix}$$

$$B_y = \begin{pmatrix} b_2^1 & b_2^2 & \cdots & b_2^N \\ b_2^1 & b_2^2 & \cdots & b_2^N \\ \vdots & \vdots & \ddots & \vdots \\ b_2^1 & b_2^2 & \cdots & b_2^N \end{pmatrix}$$

$$B_z = \begin{pmatrix} b_3^1 & b_3^2 & \cdots & b_3^N \\ b_3^1 & b_3^2 & \cdots & b_3^N \\ \vdots & \vdots & \ddots & \vdots \\ b_3^1 & b_3^2 & \cdots & b_3^N \end{pmatrix}$$

Now if we take $b_i^n = \delta_{in}$ *for* $i = 1, 2$ *and* $b_3^n = 2\delta_{3n}$ $1 \leq n \leq N$, *then:*

- $\left\{\begin{array}{l}\max \|B_x\psi\|_2^2+\|B_y\psi\|_2^2\\ \|\psi\|_2=1\end{array}\right. = \left\{\begin{array}{l}\max \psi_1^2+\psi_2^2\\ \psi_1^2+\psi_2^2+\cdots+\psi_N^2=1\end{array}\right.$ *whose solutions are all* $\psi \in \mathbb{R}^N$ *such that* $\|\psi\|_2 = 1$ *and* $\psi_3 = \cdots = \psi_N = 0$.

- $\left\{ \begin{array}{l} \max \|B_x\psi\|_2^2 + \|B_y\psi\|_2^2 + \|B_z\psi\|_2^2 \\ \|\psi\|_2 = 1 \end{array} \right. = \left\{ \begin{array}{l} \max \psi_1^2 + \psi_2^2 + 4\psi_3^2 \\ \psi_1^2 + \psi_2^2 + \cdots + \psi_N^2 = 1 \end{array} \right.$
whose solutions are all $\psi \in \mathbb{R}^N$ *such that* $\|\psi\|_2 = |\psi_3| = 1$. *Indeed,* $\psi_1^2 + \psi_2^2 + 4\psi_3^2 = 1 - \left(\psi_4^2 + \cdots + \psi_N^2\right) + 3\psi_3^2 < 4$ *if* $|\psi_3| < 1$.

Appendix C: Boundary integral equation formulation

In this work, we have used the technique developed in [14] that allows to model any divergence-free current density over a given surface. Although this approach permits different order of BEM approximation and element geometry, here it has been assumed flat triangular element geometry and linear approximation of the stream function over the element in order to model of the current under search. Thus, let us consider that the surface, $S \subseteq \mathbb{R}^3$, on which we want to find the optimal current, is divided into T triangular flat elements with N nodes, which are lying at each vertex of the element. The current density at each element can be written in terms of the nodal values of the stream function and elements of the local geometry ([14])

$$\mathbf{J}(\mathbf{r}, \psi) \approx \sum_{n=1}^{N} \psi_n \; \boldsymbol{\jmath}^n(\mathbf{r}). \tag{5.1}$$

The matrix equations that transform ψ to the various coil properties and objectives can be then constructed by incorporating the divergence-free current density model in Eq. 5.1 into the boundary integral formulations of all the magnitudes involved in the problem, that are described in the following.

5.6. Magnetic vector potential

The magnetic vector potential, $\mathbf{A}$, can be determined from

$$\mathbf{A}(\mathbf{r}) = \frac{\mu_0}{4\pi} \int_S \frac{\mathbf{J}(\mathbf{r}')}{|\mathbf{r} - \mathbf{r}'|} \, dS \tag{5.2}$$

and by applying Eq. 5.1, this yields

$$\mathbf{A}(\mathbf{r}) = \frac{\mu_0}{4\pi} \sum_{n=1}^{N} \psi_n \int_S \frac{\boldsymbol{\jmath}^n(\mathbf{r}')}{|\mathbf{r} - \mathbf{r}'|} \, dS \tag{5.3}$$

and if the conducting surface is approximated by the union of the T elements

$$\mathbf{A}(\mathbf{r}) = \frac{\mu_0}{4\pi} \sum_{n=1}^{N} \psi_n \sum_{t=1}^{T} \int_{S_t} \frac{\boldsymbol{\jmath}^n(\mathbf{r}')}{|\mathbf{r} - \mathbf{r}'|} \, dS'. \tag{5.4}$$

To simplify the notation we can write $\mathbf{A}$ as a linear combination of the magnetic potentials produced by the current element associated with each node.

$$\mathbf{A}(\mathbf{r}) = \sum_{n=1}^{N} \psi_n \mathbf{a}^n(\mathbf{r}), \tag{5.5}$$

where $\mathbf{a}^n(\mathbf{r})$ is the magnetic potential produced by a unit stream function at the nth-node [14].

5.7. Magnetic Induction

If we apply the curl operator to Eq. 5.6, an expression for the magnetic induction is then obtained

$$\mathbf{B}(\mathbf{r}) = \sum_{n=1}^{N} \psi_n \mathbf{b}^n(\mathbf{r}), \tag{5.6}$$

where $\mathbf{b}^n(\mathbf{r})$ is the magnetic induction (equivalently magnetic field) produced by a unit stream function at the nth-node [14].

5.8. Stored magnetic Energy

Operating in a similar fashion the stored magnetic energy in the TMS coil can be written as

$$W = \frac{\mu_0}{8\pi} \int_S \int_{S'} \frac{\mathbf{J}(\mathbf{r})\mathbf{J}(\mathbf{r}')}{|\mathbf{r} - \mathbf{r}'|} dS dS' = \frac{1}{2} \sum_{n=1}^{N} \sum_{m=1}^{N} \psi_n \psi_m L_{mn} \tag{5.7}$$

where L_{mn} is the mutual inductance between the m^{th} and n^{th} current elements [14]

$$L_{mn} = \frac{\mu_0}{4\pi} \int_S \int_{S'} \frac{\boldsymbol{\jmath}^n(\mathbf{r}) \cdot \boldsymbol{\jmath}^m(\mathbf{r}')}{|\mathbf{r} - \mathbf{r}'|} \, dS dS'. \tag{5.8}$$

The double integral involved in the definition of the components, L_{mn}, of the inductance matrix shows a singular behavior when $m = n$. A general approach for dealing with these type of double weak singular integrals can be found in [23], which is based on a transformation into a local polar coordinate system where the integration can be performed by avoiding the singularity.

5.9. Power dissipation

The resistive power dissipation is

$$P = \rho_{Cu} \int_S |\mathbf{J}|^2 dS = \frac{1}{2} \sum_{n=1}^{N} \sum_{m=1}^{N} \psi_n \psi_m R_{mn} \tag{5.9}$$

here R_{mn} is the resistance matrix, ρ_{Cu} the resistivity of the conducting medium (here we assumed to be copper).

5.10. Electric field

To produce an integral formulation for the electric field, we recall that there are two sources of $\mathbf{E}$, the first is the temporal derivative of the vector potential, $\mathbf{A}$, and it is produced by current flowing in the coils; the change of $\mathbf{A}$ produces initially a redistribution of free charges in the conducting

domain, which accumulate at boundaries between regions of different conductivity and generate the second, conservative contribution to **E**

$$\mathbf{E} = -\nabla\phi - \frac{\partial \mathbf{A}}{\partial t}. \tag{5.10}$$

The characterization of the magnetic component can be found in section 5.6 of the Appendix C; whereas the integral representation of conservative component of the E-field can be produced if we recall the harmonic nature of the scalar potential. Thus if a multi-compartment volume conductor D (where the ROI is included) is made of M different homogeneous sub-domains, D_i ($D = \bigcup_i^M D_i$), in each of theses subregions with uniform conductivity the scalar potential satisfies Laplace's equation.

Moreover, if we use the continuity of the current flowing at every surface between regions as a boundary condition (which is a natural or Neumann condition since the normal derivative of the potential is specified) the conservative part of the electric field at a point of the ROI2 inside the pth sub-domain system can be written as [15]

$$\frac{\partial \phi}{\partial x_j}(\mathbf{r}) = \sum_{i=0}^{M} \frac{(\sigma_i - \sigma_{i+1})}{\sigma_p} \int_{S_i} \Big[- \frac{\partial \phi^*}{\partial x_j}(\mathbf{r}, \mathbf{y}) \frac{\partial A^n}{\partial t}(\mathbf{y}) - \tag{5.11}$$
$$\frac{\partial q^*}{\partial x_j}(\mathbf{r}, \mathbf{y})\ \phi^i(\mathbf{y}) \Big] ds(\mathbf{y}), \qquad \mathbf{r} \in D_p, \qquad p = 1, ..., M.$$

where $\sigma_i,\ i = 1, ..., M$, is the conductivity of each subdomain, the Green's function dipole is given by

$$\frac{\partial \phi^*}{\partial x_j} = -\frac{x_j - y_j}{4\pi r^3}, \qquad j = 1, 2, 3, \tag{5.12}$$

and the quadrupole and is

$$\frac{\partial q^*}{\partial x_j} = -\frac{1}{4\pi} \Big[\frac{\delta_{j,k}}{r^3} - 3\frac{(x_j - y_j)(x_k - y_k)}{r^5} \Big] n_k, \qquad j = 1, 2, 3. \tag{5.13}$$

Here, we have used the tensor summation definition of the double index.

5.11. Temperature

The integral representation of the temperature above ambient, T^*, of the copper sheet can be produced by a heat equation in which the dissipation of heat throughout the object is governed by the Laplacian of T^* and heat is lost from the object by a cooling term proportional to T^*. An Ohmic heating term must be also included to take into account the power dissipated as heat energy due to $\mathbf{j}$. By assuming isotropic and uniform thermal conductivity, ignoring any non linear effects and considering the steady-state equilibrium, the heat equation that describes this problem can be written as [16]

$$\nabla^2 T^*(\mathbf{x}) - \frac{h_t}{k_e w} T^*(\mathbf{x}) = -\frac{\rho_r}{k_e w^2} \mathbf{j}(\mathbf{x}) \cdot \mathbf{j}(\mathbf{x}), \qquad \mathbf{x} \in S \tag{5.14}$$

where h_t is the total heat transfer coefficient, k_e is the effective thermal conductivity and ρ_r is the is the resistivity of the copper. Equation (5.14) for sake of simplicity, can be written as

$$\nabla^2 T^*(\mathbf{x}) - K^2 T^*(\mathbf{x}) = -c(\mathbf{x}), \qquad \mathbf{x} \in S. \tag{5.15}$$

where

$$K = \sqrt{\frac{h_t}{k_e w}}, \tag{5.16}$$

and

$$c(\mathbf{x}) = \frac{\rho_r}{k_e w^2} \mathbf{j}(\mathbf{x}) \cdot \mathbf{j}(\mathbf{x}). \tag{5.17}$$

A boundary integral representation of Eq. (5.15) can be obtained by making use of Green's second identity and the jump property of the double layer potential [16]

$$\frac{1}{2}T^*(\mathbf{x}) = \int_S c(\mathbf{y})\tau^*(\mathbf{x},\mathbf{y})dS(\mathbf{y}) - \int_S T^*(\mathbf{y})\chi^*(\mathbf{x},\mathbf{y})dS(\mathbf{y}), \qquad \mathbf{x},\mathbf{y} \in S \tag{5.18}$$

where, in order to obtain realistic solutions, Neumann boundary conditions for no heat flow in or out the surface (i.e. perfectly insulated) have been employed, $\mathbf{n} \cdot \nabla T^* = 0$; τ^* is the 3D free-space Green's function of Eq. (5.15), given by

$$\tau^*(\mathbf{x},\mathbf{y}) = \frac{1}{4\pi|\mathbf{x}-\mathbf{y}|}e^{-K|\mathbf{x}-\mathbf{y}|}, \tag{5.19}$$

and χ^* is the normal derivative of the free-space Green's function

$$\chi^*(\mathbf{x},\mathbf{y}) = \frac{\partial\tau^*}{\partial n} = \frac{(\mathbf{x}-\mathbf{y})\cdot\mathbf{n}}{4\pi|\mathbf{x}-\mathbf{y}|^3}\; e^{-K|\mathbf{x}-\mathbf{y}|}\big(1-K|\mathbf{x}-\mathbf{y}|\big). \tag{5.20}$$

The current characterization, Eq. (5.1), is now incorporated in Eq. (5.17), the Joule heating coefficient at the k-element can be written as

$$c_k = \frac{\rho_r}{k_e w^2}\mathbf{j}(\mathbf{x})\cdot\mathbf{j}(\mathbf{x}) = \frac{\rho_r}{k_e w^2}\sum_{n=1}^{N}\varphi_n\;\boldsymbol{\jmath}^n(\mathbf{x})\cdot\sum_{m=1}^{N}\varphi_m\;\boldsymbol{\jmath}^m(\mathbf{x}), \qquad \mathbf{x}\in S_k. \tag{5.21}$$

The discretized version of Eq. (5.18) can be finally written

$$\frac{1}{2}T^*(\mathbf{x}) + \sum_{k=1}^{L}\int_{S_k} T^*(\mathbf{y})\;q^*(\mathbf{x},\mathbf{y})\;ds(\mathbf{y}) = \sum_{k=1}^{L}\int_{S_k}\phi^*(\mathbf{x},\mathbf{y})\;c(\mathbf{y})\;ds(\mathbf{y}), \qquad \mathbf{x},\mathbf{y}\in S. \tag{5.22}$$